Chinese Chemical Letters 35 (2024) 108692

Contents lists available at ScienceDirect

Chinese Chemical Letters

journal homepage: www.elsevier.com/locate/cclet

Modulating the degree of O vacancy defects to achieve selective control of electrochemical CO_2 reduction products

Tianbo Jia[a,1], Lili Wang[b,1], Zhouhao Zhu[c], Baikang Zhu[a,c], Yingtang Zhou[a,*], Guoxing Zhu[d,*], Mingshan Zhu[e], Hengcong Tao[a,c,**]

[a] School of Petrochemical Engineering & Environment, Zhejiang Ocean University, Zhoushan 316022, China
[b] Department of General Practice, First Medical Center, Chinese PLA General Hospital, Beijing 100853, China
[c] National & Local Joint Engineering Research Center of Harbor Oil & Gas Storage and Transportation Technology, Zhoushan 316022, China
[d] School of Chemistry and Chemical Engineering, Jiangsu University, Zhenjiang 212013, China
[e] Guangdong Key Laboratory of Environmental Pollution and Health, School of Environment, Jinan University, Guangzhou 511443, China

ARTICLE INFO

Article history:
Received 12 May 2023
Revised 5 June 2023
Accepted 13 June 2023
Available online 20 June 2023

Keywords:
CO_2
O-vacancies
Bimetallic catalysts
Copper oxide
Cadmium oxide
Selective

ABSTRACT

Conversion of CO_2 into high-value products using electrochemical CO_2 reduction (ECR) technology is an effective way to alleviate global warming and reach carbon neutrality. The oxygen vacancies in heterogenous catalysis are generally considered as a powerful method to enhance the performance of ECR by promoting CO_2 adsorption and activation. However, the extent of defects in oxygen vacancies-activity relation has rarely been studied. Herein, we prepared Cu–Cd bimetallic catalysts with adjustable oxygen defect degree by controlling the amount of cadmium addition. Fourier transform infrared spectroscopy characterization results reveal that the formation of oxygen vacancies is attributed to the asymmetric stretching of Cu–O by the addition of cadmium. Electrochemical results show that the oxygen defect degree can modulate the selectivity of ECR products. A low degree of oxygen defects (CuO) is generally associated with lower product Faraday efficiency ($FE_{C2}/FE_{C1} \approx 114\%$), but overabundant oxygen vacancies ($CuO_{2.625}$–$CdO_{0.375}$) are not entirely favorable to improving ECR activity ($FE_{C2}/FE_{C1} \approx 125\%$) and single selectivity, while an appropriate degree of oxygen vacancies ($CuO_{2.75}$–$CdO_{0.25}$) can facilitate the ECR process toward single product selective production ($FE_{C2}/FE_{C1} \approx 296\%$). The theoretical calculation showed that the O vacancy formed on CuO and the interface between CdO and CuO were conducive to enhancing the formation of *COOH intermediate and promoting the generation of ethylene products. This study provides a new approach and insight into the selective production of single products for future industrial applications of ECR.

Global warming due to rising atmospheric CO_2 concentrations and several resulting negative impacts are among the global challenges of the past and future decades [1,2]. Among the numerous CO_2 treatment technologies, electrochemical CO_2 reduction (ECR) is considered a promising technology for mitigating global warming, reducing reliance on fossil fuels, and promoting the artificial carbon cycle [3], as it uses green and renewable electricity to drive the conversion of CO_2 into valuable chemicals including CO, CH_4, C_2H_4, and alcohols [4–6]. In recent years, a large number of metal catalysts have been developed for use in ECR processes, and these metals can be broadly classified into four categories: (1) Hg, Tl, In, and Bi from which HCOOH is the major product; (2) Au, Ag, Zn, Pd, and Ga with CO as the main product; (3) Ni, Fe, Pt, and Ti primarily producing H_2; and (4) Cu, because it is a metal with negative sorption energy for *CO and positive sorption energy for *H, Cu is the only metal that can convert CO_2 to hydrocarbons, and its suitable desorption energy makes Cu-based catalysts unique in the ECR process [7–9]. However, the Cu-based materials reported thus far have three main obstacles to the efficient conversion of CO_2 to ethylene (C_2H_4): (1) More violent hydrogen precipitation reactions at too high a potential; (2) a strong energy barrier to the C-C coupling reaction and (3) competition between C-O and C-H [10].

However, considering that the ECR process is usually accompanied by the formation of C1 products, C2 products, and H_2, it is often difficult to control the high selectivity for the target products

* Corresponding authors.
** Corresponding author at: School of Petrochemical Engineering & Environment, Zhejiang Ocean University, Zhoushan 316022, China.
E-mail addresses: zhouyingtang@zjou.edu.cn (Y. Zhou), zhuguoxing@ujs.com.cn (G. Zhu), hengcongtao@zjou.edu.cn (H. Tao).
[1] These authors contributed equally to this work.

https://doi.org/10.1016/j.cclet.2023.108692
1001-8417/

with pure Cu catalysts [11]. Therefore, a large number of strategies have been used to enhance the selectivity of Cu-based catalysts for single products, such as heteroatom doping [12–15], modulation of nanoparticle size [16,17], forming bimetallic catalysts [10,18-20], crystal plane control [21,22]. Among all these strategies, the formation of bimetallic catalysts is one of the most frequently used strategies for the engineering of vacancies and defects [23]. Bimetallic catalysts occupy a unique position because their specific electronic properties differ from those of the corresponding constituent metals [24], while the abundance of defects in the vicinity of vacancies allows chemisorption and stabilization of critical reaction intermediates for the subsequent generation of target products [25,26]. However, the O vacancy has the disadvantage of being unstable, and the degree of defect is difficult to regulate, which makes it difficult to achieve efficient and selective conversion of target products. It is worth noting that if the defect degree of O vacancies can be effectively controlled, selective regulation of reaction products can be achieved.

In recent years, CdO has been reported to be widely used in photocatalysis [27,28], biological antibacterial materials [29], gas sensors [30], dielectric [31], *etc*., but there are relatively few reports on the use of CdO for ECR. CdO has been chosen to build interfaces with high thermal stability, excellent CO_2 adsorption properties, and low cost. In addition, CdO is also a good metal oxide for forming O vacancies theoretically [32,33], so the strategy of controlling the O defect degree of CuO by using CdO is very valuable research.

In this study, we demonstrate the synthesis of a simple CuO-CdO bimetallic electrocatalyst with a large-scale and intimate contact interface. Electrochemical tests show that the resulting product contains CO, CH_4, C_2H_4, and H_2. Selective conversion of the product can be achieved by adjusting the amount of CdO added and controlling the extent of defective O vacancies. The Cu–Cd bimetallic catalyst in 0.1 mol/L $KHCO_3$ electrolyte has the best ethylene selectivity at a Cu/Cd molar ratio of 11/1 ($CuO_{2.75}$-$CdO_{0.25}$), with $FE_{C_2H_4}$ reaching 55.4% at −1.2 V (*vs.* reversible hydrogen electrode (RHE)), pure CdO exhibiting more than 88% FE_{CO}, and a series of Cu-Cd bimetallic catalysts only. This work provides a new and feasible idea for future selective conversion of CO_2 to a single product by adjusting the degree of defect in the O vacancy.

X-ray diffraction measurements were carried out to investigate the phases of the products (Fig. 1a). The bimetallic catalysts consisted mainly of CuO and CdO, which was confirmed by peaks at 32.5°, 35.4°, 35.5°, 38.7°, 38.9°, 48.7°, 53.5°, 58.3°, 61.5°, 65.8°, 66.2° and 68.1° for the CuO(110), (002), (11$\bar{1}$), (111), (200), (20$\bar{2}$), (020), (202), (11$\bar{3}$), (31$\bar{1}$) and (220) planes (JCPDS No. 48-1548) and peaks at 33.0°, 38.3°, 55.3°, 65.9° and 69.3° for the CdO (111), (200), (220), (311), and (222) planes (JCPDS No. 05-0640), respectively.

The FTIR spectrum shown in Fig. 1b clearly shows asymmetric stretching vibrations at 1404 cm^{-1}, which can be attributed to asymmetric stretching vibrations between Cu–O–Cd. To confirm the presence of vacancy O in CuO-CdO, ESR tests (Fig. 1c) were performed on CuO, CdO and $CuO_{2.75}$-$CdO_{0.25}$. $CuO_{2.75}$-$CdO_{0.25}$ was found to exhibit strong symmetry at $g \approx 2.0$, stronger than CuO and CdO. Unpaired electrons are captured through oxygen vacancies by the adsorption of oxygen molecules from air. Fig. 1d shows that $CuO_{2.75}$-$CdO_{0.25}$ has the highest CO_2 adsorption capacity, indicating that it may have more active sites for CO_2 adsorption and that an excess of O vacancies could instead lead to unfavorable CO_2 adsorption. This result suggests that an asymmetric interface containing the appropriate level of O vacancy defects is most favorable for the adsorption of CO_2 products, in agreement with recent findings that have been reported [34]. The wide scan XPS spectrum in Fig. S1 (Supporting information) shows the characteristics of Cu, Cd, O, and C. Fig. 1e shows the Cu 2p XPS spectra of CuO-CdO catalysts with different molar ratios. The Cu species in

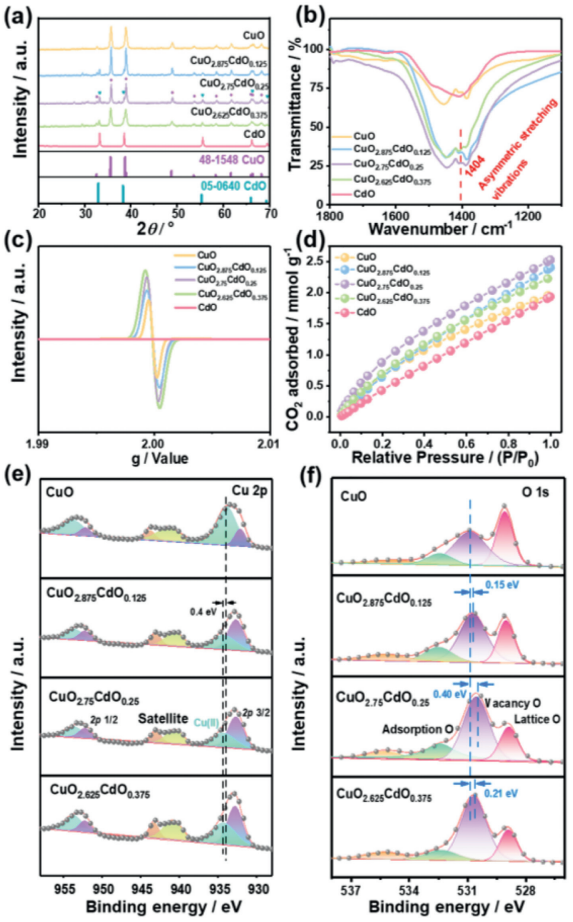

Fig. 1. (a) XRD patterns, (b) FT-IR spectra, (c) ESR spectra, (d) CO_2 desorption curves, (e) Cu 2p XPS spectra, and (f) O 1s XPS spectra of the Cu-Cd bimetallic catalyst.

pure CuO consisted of Cu^{2+} $2p_{3/2}$ at ~934.4 eV and a very small amount of $Cu^{0/+}$ at ~932.7 eV. The proportion of $Cu^{0/+}$ in the Cu species appears to increase more significantly after the addition of CdO, implying an increase in the electron self-density around the Cu atom. It is noteworthy that no Cu species are evident in the pure CdO catalyst. The O 1s spectrum is deconvolved into three peaks located (Fig. 1f) at ~532.4 eV, ~531.5 eV, and ~528.9 eV. In the present work, the peak centered at 532.4 eV is attributed to O in physisorbed H_2O [35], assigned to an O defect or vacant state at 531.5 eV [36]. We found that $CuO_{2.625}$–$CdO_{0.375}$ had the highest O vacancy percentage of 81.03% > 72.34% for $CuO_{2.75}$–$CdO_{0.25}$ > 67.94% for $CuO_{2.875}$–$CdO_{0.125}$ > 55.95% for CuO (Fig. S2 in Supporting information), which is also consistent with the ESR spectrum. The peaks at 528.9 eV are due to O binding to metals (Cu-O) [37]. Compared to CuO, the Cu 2p in CuO-CdO slightly positively shifted (Fig. 1e) and the O 1s slightly negatively shifted (Fig. 1f), indicating that the addition of CdO significantly modulates the electronic structure of CuO. The Cu $2p_{3/2}$ of CuO-CdO is positively shifted by 0.40 eV compared to CuO, while the O 1s peaks show negative shifts of 0.15, 0.40 and 0.21 eV. These shifts indicate that charge transfer interactions between Cu and O atoms have occurred. The Cd XPS spectrum shows Cd^{2+} as the major component and two peaks at 411.1 and 404.4 eV corresponding to Cd $3d_{3/2}$ and Cd $3d_{5/2}$ respectively [38], while the low-intensity peak at 406.6 eV can be attributed to a very small amount of $CdCO_3$ (Fig. S3 in Supporting information) [39].

To clearly distinguish between several catalysts in the series, scanning electron microscopy (SEM) (Fig. 2a and Figs. S4a-d

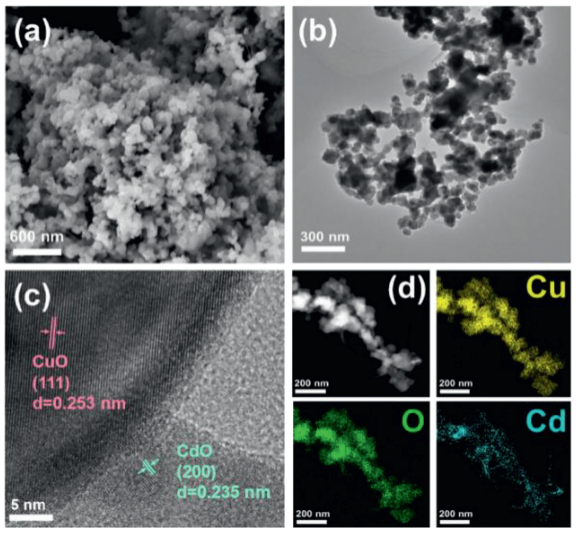

Fig. 2. (a) SEM, (b) TEM, (c) HRTEM, and (d) EDS image of $CuO_{2.75}$-$CdO_{0.25}$.

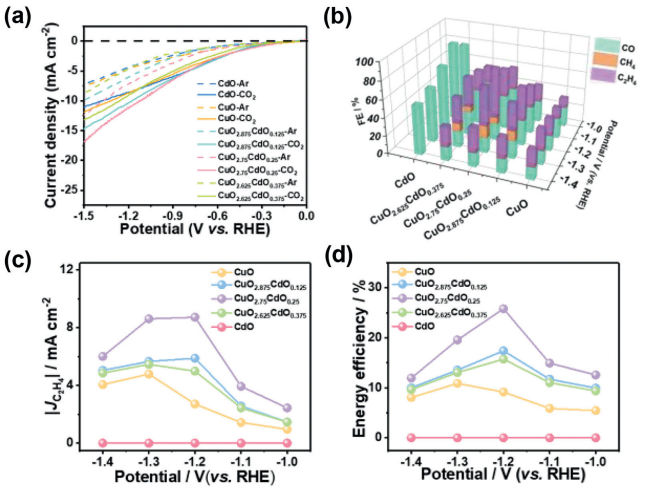

Fig. 3. (a) LSV curves in Ar and CO_2 for Cu-Cd bimetallic catalysts at a scan rate of 10 mV/s and (b) ECR FE over Cu–Cd bimetallic catalyst electrode in CO_2-purged 0.1 mol/L $KHCO_3$ at different applied potentials. (c) C_2H_4 partial geometric current density ($|jC_2H_4|$) for different electrocatalysts and (d) C_2H_4 cathodic EE of Cu–Cd bimetallic catalysts at different applied potentials.

in Supporting information) and transmission electron microscopy (TEM) imaging (Fig. 2b) were performed on Cu-Cd bimetallic catalysts. There is no major difference in the morphological structure of the Cu–Cd bimetallic catalysts, with regularly sized nanoparticles in a closely arranged massive structure and a rough surface. High-resolution TEM (HR-TEM) (Fig. 2c) revealed that CuO and CdO are highly crystalline with ordered lattice fringes. Further HR-TEM images (Fig. S5 in Supporting information) show a clear interfacial connection between CuO and CdO, indicating the formation of a heterogeneous structure between CuO and CdO. This corresponds in part to the XRD results and the energy dispersive X-ray spectroscopy (EDS) elemental mapping (Fig. 2d) showing that Cu, O, and Cd elements are evenly distributed on the pellet, which also indicates that no alloy structure is formed between Cu and Cd. The molar ratios of the Cu-Cd bimetallic catalysts were obtained by ICP-OES (Table S1 in Supporting information) and showed that the molar ratios matched the feed ratios, which is consistent with the EDS elemental mapping results (Fig. 2d).

The electrochemical performance of Cu-Cd bimetallic catalysts was investigated in a three-electrode H-type closed electrolyzer containing 0.1 mol/L $KHCO_3$ (Fig. S6 in Supporting information). Linear scanning voltammetry (LSV) results (Fig. 3a) have shown that the current density in the CO_2 environment is greater than that in the Ar environment within a voltage range of 0 V to −1.5 V (*vs.* RHE). Notably, $CuO_{2.75}$–$CdO_{0.25}$ obtained the highest current densities compared to the other investigated materials across the entire tested potential range. Gas chromatography (GC) and nuclear magnetic resonance (NMR) were used to detect the gas phase and liquid phase products of the Cu–Cd bimetallic catalyst after 1 h constant voltage electrochemical test. The gas phase products mainly include H_2, CO, CH_4, and C_2H_4. The yields of the liquid phase products are negligibly small (Fig. S7 in Supporting information). Pure CuO exhibited a certain ability to produce C_2H_4, but its FE was low and $FE_{C_2H_4}$ increased with increasing CdO content, reaching a maximum at $CuO_{2.75}$–$CdO_{0.25}$. A further increase in the amount of CdO leads to a decrease in the ECR activity, most likely due to the addition of large amounts of CdO reducing the surface Cu active site, while the Cd active site produces more C1 products and even pure CdO generates large amounts of CO (Fig. 3b). Combined with the ESR spectroscopy results, we conclude that the selectivity of ECR products is closely related to the degree of O vacancy defects; specifically, a moderate degree of O defects helps to enhance the selectivity of the catalyst for C_2H_4 during ECR, and either too high or too low O defect ranges are detrimental to the production of C_2H_4 products. The highest $FE_{C_2H_4}$ of 55.4% was produced by $CuO_{2.75}$-$CdO_{0.25}$ at −1.2 V (*vs.* RHE) approximately 2.3, 1.5, and 1.7 times than that of CuO, $CuO_{2.875}$–$CdO_{0.125}$, and $CuO_{2.625}$–$CdO_{0.375}$, respectively. Interestingly, we observed that the addition of CdO reduced the potential to produce the best $FE_{C_2H_4}$ from −1.3 V to −1.2 V. Figs. 3c and d show the special current density and energy efficiency (EE) of ethylene after optimization of Cu-Cd bimetallic catalysts. $CuO_{2.75}$–$CdO_{0.25}$ delivers a maximal $EE_{C_2H_4}$ of ~25.9% at a current density of 8.8 mA/cm^2. Notably, the $FE_{C_2H_4}$ or low applied potential demonstrated by $CuO_{2.75}$–$CdO_{0.25}$ exceeded many of the existing Cu-based materials in similar reports (Fig. S8 and Table S2 in Supporting information) [10,26,40-47]. In addition, $CuO_{2.75}$–$CdO_{0.25}$ provides better selectivity ($FE_{C_2H_4}/FE_{C1} \approx 3$) and C_2H_4 production rate (maximum ~16.4 μmol mg^{-1} h^{-1}) of C_2H_4 products than pure CuO catalysts or other molar ratios of Cu–Cd bimetallic catalysts over a wide voltage range of −1.0 V to −1.4 V (*vs.* RHE) (Figs. S9 and S10 in Supporting information).

The selective enhancement can be attributed primarily to the varying degrees of O defects formed by the stretching action of CdO on CuO rather than to the commonly assumed change in the electronic properties of the interface. Since the high CdO content ($CuO_{2.625}$–$CdO_{0.375}$) has a greater interfacial electronic property change, but its ethylene product selectivity shows a decreasing trend, which is not as convincing as expected, we believe that there is a limit to the O vacancies formed by CdO stretching in enhancing the catalytic performance and that an appropriate degree of defects is favorable for the production of ethylene products.

To obtain a deeper understanding of the activity and mechanism of different catalysts on ECR catalysts, the double-layer capacitance (C_{dl}) of each catalyst in this study was tested by CV to obtain the electrochemically active surface area (ECSA) of each sample (Figs. S11a-e in Supporting information) [48]. As shown in Fig. S10a, $CuO_{2.75}$–$CdO_{0.25}$ exhibits the highest ECSA, suggesting that $CuO_{2.75}$–$CdO_{0.25}$ provides more active sites for ECR, increasing the opportunity for intermediates to bind at the interface with the electrolyte [49]. The charge transfer rates between the catalyst and electrolyte interfaces were characterized by electrochemical impedance spectrum (EIS) (Fig. S12 in Supporting information). The results show that the half-circle diameter of Nyquist with

$CuO_{2.75}$–$CdO_{0.25}$ is less than that with $CuO_{2.875}$–$CdO_{0.125}$, $CuO_{2.625}$–$CdO_{0.375}$, CuO, and CdO, indicating that it has a faster realization of electron transfer [50,51]. The Tafel slope of the Cu-Cd bimetallic catalyst is shown in Fig. S13 (Supporting information). The Tafel slope was used to measure the reaction kinetics of the four catalysts, with the lowest Tafel slope (340.2 mV/dec) for $CuO_{2.75}$–$CdO_{0.25}$, implying the lowest kinetic energy required to activate the CO_2. In addition, the continuous ECR experiments at −1.2 V (*vs.* RHE) resulted in almost no decrease in $FE_{C_2H_4}$ within 11 h, indicating that the catalyst has good electrochemical stability (Fig. S14 in Supporting information).

DFT was employed to further explore the potential mechanism of ECR of Cu-Cd bimetallic catalysts. First, based on X-ray diffraction (CuO with JCPDS No. 48-1548 and CdO with JCPDS No. 05-0640) and HRTEM, the unit structures models of CuO and CdO are shown in Fig. S15 (Supporting information). CuO consists of 4 Cu and 4 O atoms with a space group of C2/c and a lattice length of 4.70 Å × 4.70 Å × 4.70 Å. CdO consists of four Cd and four O atoms with a space group of Fm-3 m and a lattice length of 4.69 Å × 3.42 Å × 5.13 Å. The heterojunction CuO–CuO consists of CuO(111) and CdO(200) with a lattice mismatch of less than 5%, demonstrating the excellent suitability of CuO(111) and CdO(200). The O atoms were removed according to the ratio of XPS results from the CuO–CuO surface to represent O vacancy.

Generally, the production of ethylene by ECR involves five steps, first CO_2 adsorption at the active site to form $*CO_2$ (step 1), followed by the formation of *COOH and *CO or intermediates on the catalyst surface (steps 2 and 3), followed by the formation of *CHO intermediates (step 4), and finally the coupling of *CO or *CHO to form ethylene [26]. The formation of *CO during the above process is crucial for ethylene production [52]. Therefore, we subsequently investigated the free energies of conversion of *COOH and *CO on the CuO–CuO and CuOv–CdO surfaces. The free energies and corresponding relaxed structures were shown in Figs. 4a-c and Table S3 (Supporting information). The lower reaction potential barrier of CuOv-CdO indicates that it is more efficient to generating the *COOH intermediate, thus increasing the efficiency of the *CO intermediate and the efficiency of ethylene production. For the optimized structures, only C and Cu are bonded during the *COOH adsorption of CuO–CdO, however, the oxygen vacancy of CuOv-CdO attracts the O atom of the *COOH intermediate. The oxygen vacancy on the CuO–CdO subsurface lowers potential determing step from *CHO to *COCHO in ECR process with the energy barrier CuOv-CdO (1.37 eV) and CuO–CdO (1.46 eV), reducing the overpotentials and thus promoting ECR activity (Fig. S16 in Supporting information).

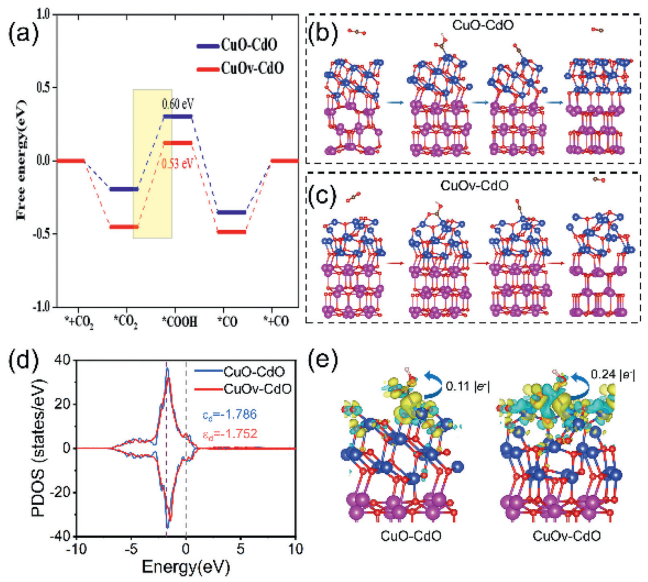

Fig. 4. (a) Free energy diagram for CO on CuO-CdO and CuOv-CdO. (b, c) The optimized configurations of intermediates on the surface of CuO-CdO and CuOv-CdO. (d) Projected density of states and d-band center of the d orbitals of Cu for CuO-CuO and CuOv-CdO. (e) Charge density difference and Bader charge of *COOH intermediate on the surface of CuO-CdO and CuOv-CdO.

To further explore the mechanism of enhanced ethylene production efficiency by CuOv-CdO, we calculated the projected density of states and d-band center of the d orbitals of Cu for CuO–CuO and CuOv–CdO (Fig. 4d). The d orbitals of Cu for CuOv–CdO move toward the Fermi level, indicating the activation of Cu. Generally, the approach of the d-band center to the Fermi level indicates that transition metal catalysts are more likely to exhibit high adsorption activity [53,54]. The d-band center of CuOv-CdO was closer to the Fermi level than that of CuO–CuO (−1.752 *vs.* −1.786), indicating the adsorption activity of CuOv-CdO. CuOv–CdO showed an increased adsorption activity of Cu, thus improving and facilitating the chemisorption of reaction intermediates on the catalytic surface. The charge density difference and Bader charge were employed to reveal the mechanism of the high adsorption of *COOH on CuOv–CdO. As shown in Fig. 4e, yellow represents charge aggregation and cyan represents charge dissipation. CuOv–CdO showed more significant charge transfer with *COOH than the CuO–CuO surface and transferred more charge (0.24 $|e^-|$ *vs.* 0.11 $|e^-|$), with more charge transfer indicating that the oxygen vacancies increased the adsorption of *COOH and lowered the reaction potential. Therefore, the increasing charge transfer indicates that the oxygen vacancies increase the adsorption of *COOH and lower the reaction potential, thus increasing the yield of ethylene.

In situ Raman measurements were performed to further confirm the excellent ECR performance of CuO-CdO materials. As shown in Fig. S17 (Supporting information), the $CuO_{2.75}$–$CdO_{0.25}$ electrode shows a peak at 360 cm^{-1}, corresponding to the stretching of Cu-CO [55]. Furthermore, the enhancement of the intensity at 1045 cm^{-1} compared to the open circuit potential (OCP) can be attributed to *COOH [26]. Combined with the DFT results, we can assume that the presence of O vacancies enhances the ability of the catalyst surface to adsorb *COOH. The peak at 515 cm^{-1} is assigned to the OH group with improved charge balance [56], which can improve the charge balance to enhance C_2H_4 selectivity.

To study the stability of the catalysts, the catalysts used were characterized by XPS and TEM, the results of which are shown in Figs. S18-S21 (Supporting information). In general, the species of Cu and Cd did not change significantly, while the ratio of O vacancies was different from that of fresh, which may be due to *in situ* reduction and air oxidation during the reaction. The good stability of $CuO_{2.75}$–$CdO_{0.25}$ was further confirmed by the negligible variation in its TEM and EDS mapping after electrolysis.

In summary, we have demonstrated for the first time a low-cost and easily prepared bimetallic catalyst of CuO and CdO for the electrochemical CO_2 reduction to C_2H_4, which can provide 55.4% of $FE_{C_2H_4}$ at −1.2 V (*vs.* RHE). It is 2.3 times more than the pure CuO catalyst prepared by the same method and possesses an electrochemical stability of more than 10 h. The characterization results showed that the $CuO_{2.75}$–$CdO_{0.25}$ bimetallic catalyst formed by CdO loading on CuO particles exhibited excellent performance. The experimental results showed that the addition of CdO not only facilitated the adsorption of CO_2 by CuO but also CdO could produce abundant O defects in CuO. The degree of defective O vacancy can be controlled by changing the content of CdO to further change the product selectivity. We propose that the degree of O vacancies defects correlates with the selectivity of the products of the ECR process and that a moderate degree of O vacancy defects facilitates the conversion of CO_2 to C_2H_4, while excess O vacancies are detri-

mental to the adsorption of CO_2, leading to a decrease in its selectivity. The DFT results and *in-situ* Raman spectrum confirmed that the oxygen vacancy of CuOv–CdO leads to a lower reaction potential for the generation of *COOH intermediates and thus increases the efficiency of C_2H_4 production. This study provides a new and feasible idea for the future selective production of ECR on an industrial scale by regulating the degree of O vacancy defects.

Declaration of competing interest

The authors declare that they have no known competing financial interests or personal relationships that could have appeared to influence the work reported in this paper.

Acknowledgments

This research was funded by the National Natural Science Foundation of Zhejiang Province (Nos. LQ21B030007 and LTGS23B030002), "Leading Goose" R&D Program of Zhejiang (No. 2023C01191); the National Natural Science Foundation of China (No. 22005269), Science and Technological program of Ningbo (No. 2021S136), The Open Research Subject of Zhejiang Key Laboratory of Petrochemical Environmental Pollution Control (No. 2022Z02).

Supplementary materials

Supplementary material associated with this article can be found, in the online version, at doi:10.1016/j.cclet.2023.108692.

References

[1] I. Merino-Garcia, J. Albo, J. Solla-Gullon, et al., J. CO_2 Util. 31 (2019) 135–142.
[2] X. Zhang, Z. Zhang, H. Li, et al., Adv. Energy Mater. 12 (2022) 2201461–2201488.
[3] J. Gao, W. Tian, H. Zhang, Tungsten 4 (2022) 284–295.
[4] X. Chen, J. Chen, N.M. Alghoraibi, et al., Nat. Catal. 4 (2021) 20–27.
[5] K. Xu, S. Zheng, Y. Li, et al., Chin. Chem. Lett. 33 (2022) 424–427.
[6] J. He, X. Wang, S. Jin, et al., Chin. J. Catal. 43 (2022) 1306–1315.
[7] S. Nitopi, E. Bertheussen, S.B. Scott, et al., Chem. Rev. 119 (2019) 7610–7672.
[8] D. Raciti, C. Wang, ACS Energy Lett. 3 (2018) 1545–1556.
[9] A. Bagger, W. Ju, A.S. Varela, et al., ChemPhysChem 18 (2017) 3266–3273.
[10] X. Li, L. Li, L. Wang, et al., Chem. Commun. 58 (2022) 7412–7415.
[11] T. Jia, L. Wang, L. Zhang, et al., Surf. Interfaces (2023) 102841.
[12] Q. Wan, J. Zhang, B. Zhang, et al., Green Chem. 22 (2020) 2750–2754.
[13] Z. Liang, T. Zhuang, A. Seifitokaldani, et al., Nat. Commun. 9 (2018) 205–213.
[14] Y. Zhou, F. Che, M. Liu, et al., Nat. Chem. 10 (2018) 974–980.
[15] S. Kaur, M. Kumar, D. Gupta, et al., Nano Energy 109 (2023) 108242.
[16] I. Merino-Garcia, J. Albo, A. Irabien, Nanotechnology 29 (2017) 014001–014016.
[17] Y. Bu, M. Zhao, G. Zhang, et al., Chem. Electro. Chem. 6 (2019) 1831–1837.
[18] X. Su, Y. Sun, L. Jin, et al., Appl. Catal. B 269 (2020) 118800–118808.
[19] L. Hou, J. Han, C. Wang, et al., Inorg. Chem. Front. 7 (2020) 2097–2106.
[20] B. Ren, Z. Zhang, G. Wen, et al., Adv. Mater. 34 (2022) 2204637.
[21] G.L. De Gregorio, T. Burdyny, A. Loiudice, et al., ACS Catal. 10 (2020) 4854–4862.
[22] Y. Wu, C. Chen, X. Yan, et al., Green Chem. 22 (2020) 6340–6344.
[23] D. Ren, Y. Deng, A.D. Handoko, et al., ACS Catal. 5 (2015) 2814–2821.
[24] J. Zhang, Y. Wang, H. Wang, et al., Chin. Chem. Lett. 33 (2022) 2065–2068.
[25] M. Wang, Q. Zhang, Q. Xie, et al., Nanoscale 12 (2020) 17013–17019.
[26] P. Guo, Z. He, S. Yang, et al., Green. Chem. 24 (2022) 1527–1533.
[27] G. Wang, W. Tang, C. Xu, et al., Appl. Surf. Sci. 599 (2022) 153960–153968.
[28] G. Wang, L. Gong, Z. Li, et al., Phys. Chem. Chem. Phys. 22 (2020) 9587–9592.
[29] G. Somasundaram, J. Rajan, J. Paul, Toxicol. Res. 7 (2018) 779–791.
[30] K. Choudhary, R. Saini, G.K. Upadhyay, et al., J. Alloys Compd. 879 (2021) 160479–160486.
[31] A. Akouibaa, R. Masrour, A. Jabar, et al., Opt. Quantum. Electron. 53 (2021) 1–20.
[32] M. Liu, Y. Wang, D. Lu, J. Mater. Sci. 54 (2019) 3354–3367.
[33] Y. Ding, Y. Wang, L. Zhang, et al., J. Mater. Sci. 22 (2012) 980–986.
[34] S. Qiao, Y. Chen, Y. Tang, et al., Chem. Eng. J. 454 (2023) 140321–140330.
[35] M. Ma, C. Oh, J. Kim, et al., Appl. Catal. B 259 (2019) 118095–118104.
[36] M. Xu, Y. Chen, J. Qin, et al., Environ. Sci. Technol. 52 (2018) 13879–13886.
[37] J. Lu, J. Wang, Q. Zou, et al., ACS Catal. 9 (2019) 2177–2195.
[38] S. Ma, Y. Deng, J. Xie, et al., Appl. Catal. B 227 (2018) 218–228.
[39] S. Lee, J. Han, H.M. Ro, Chemosphere 287 (2022) 132179–132188.
[40] S. Chu, X. Yan, C. Choi, et al., Green Chem. 22 (2020) 6540–6546.
[41] Z. Chang, S. Huo, W. Zhang, et al., J. Phys. Chem. C 121 (2017) 11368–11379.
[42] S. Jia, Q. Zhu, H. Wu, et al., Chin. J. Catal. 41 (2020) 1091–1098.
[43] D. Chen, Y. Wang, D. Liu, et al., Carbon Energy 2 (2020) 443–451.
[44] Y. Liu, X. Fan, A. Nayak, et al., Proc. Natl. Acad. Sci. U. S. A. 116 (2019) 26353–26358.
[45] D. Wu, C. Dong, D. Wu, et al., J. Mater. Chem. A 6 (2018) 9373–9377.
[46] P. De Luna, R. Quintero-Bermudez, C.T. Dinh, et al., Nat. Catal. 1 (2018) 103–110.
[47] X. Qiu, H. Zhu, J. Huang, et al., J. Am. Chem. Soc. 143 (2021) 7242–7246.
[48] L. Ling, C. Yuan, Q. Xu, et al., Surf. Interfaces 36 (2023) 102483–102491.
[49] W. Zhang, L. Ding, W. Sun, et al., Inorg. Chem. 60 (2021) 14371–14381.
[50] Q. Chen, C. Yuan, C. Zhai, Chin. Chem. Lett. 33 (2022) 983–986.
[51] Y. Long, H. Xu, J. He, et al., Surf. Interfaces 31 (2022) 102056–102063.
[52] S. Ma, M. Sadakiyo, M. Heima, et al., J. Am. Chem. Soc. 139 (2017) 47–50.
[53] M. Mavrikakis, B. Hammer, J.K. Nørskov, Phys. Rev. Lett. 81 (1998) 2819–2823.
[54] Z. Zhu, H. Tao, J. Fu, et al., Chin. Chem. Lett. 34 (2023) 107476.
[55] X. Yan, C. Chen, Y. Wu, et al., Chem. Sci. 12 (2021) 6638–6645.
[56] L. Zhang, X. Li, L. Chen, et al., J. Colloid Interface Sci. 640 (2023) 783–790.